





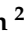
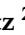





Article

Structure, Optical and Magnetic Properties of Two Isomeric 2-Bromomethylpyridine Cu(II) Complexes [Cu(C₆H₉NBr)₂(NO₃)₂] with Very Different Binding Motives

Fatma Garci ^{1,2} , Hammouda Chebbi ^{1,3,*} , Nahal Rouzbeh ⁴ , Leonhard Rochels ⁴ , Sabrina Disch ⁴ , Alexander Haseloer ² , Sean S. Sebastian ² , Uwe Ruschewitz ² , Eric Tobeckukwu Anthony ² , Axel Klein ^{2,*}  and Mohamed Faouzi Zid ^{1,*} 

- ¹ University of Tunis El Manar, Faculty of Sciences of Tunis Laboratory of Materials, Crystal Chemistry and Applied Thermodynamics, El Manar II, Tunis 2092, Tunisia
 - ² University of Cologne, Faculty of Mathematics and Natural Sciences, Department of Chemistry, Institute for Inorganic Chemistry, Greinstrasse 6, D-50939 Köln, Germany
 - ³ University of Tunis, Preparatory Institute for Engineering Studies of Tunis, Jawaharlal Nehru Street, Montfleury, Tunis 1089, Tunisia
 - ⁴ University of Cologne, Faculty of Mathematics and Natural Sciences, Department of Chemistry, Institute for Physical Chemistry, Greinstrasse 4–6, D-50939 Köln, Germany
- * Correspondence: chebbamouda@yahoo.fr (H.C.); axel.klein@uni-koeln.de (A.K.); medfaouzi.zid57@gmail.com (M.F.Z.)

Abstract: Two isomeric 2-bromomethylpyridine Cu(II) complexes [Cu(C₆H₉NBr)₂(NO₃)₂] with 2-bromo-5-methylpyridine (L¹) and 2-bromo-4-methylpyridine (L²) were synthesized as air-stable blue materials in good yields. The crystal structures were different with [Cu(L¹)₂(NO₃)₂] (**CuL¹**) crystallizing in the monoclinic space group *P*2₁/*c*, while the 4-methyl derivative **CuL²** was solved and refined in triclinic *P* $\bar{1}$. The orientation of the Br substituents in the molecular structure (*anti* (**CuL¹**) vs. *syn* (**CuL²**) conformations) and the geometry around Cu(II) in an overall 4 + 2 distorted coordination was very different with two secondary (axially elongated) Cu–O bonds on each side of the CuN₂O₂ basal plane in **CuL¹** or both on one side in **CuL²**. The two Br substituents in **CuL²** come quite close to the Cu(II) centers and to each other (Br ··· Br ~3.7 Å). Regardless of these differences, the thermal behavior (TG/DTA) of both materials is very similar with decomposition starting at around 160 °C and CuO as the final product. In contrast to this, FT-IR and Raman frequencies are markedly different for the two isomers and the UV–vis absorption spectra in solution show marked differences in the π – π^* absorptions at 263 (**CuL²**) or 270 (**CuL¹**) nm and in the ligand-to-metal charge transfer bands at around 320 nm which are pronounced for **CuL¹** with the higher symmetry at the Cu(II) center, but very weak for **CuL²**. The *T*-dependent susceptibility measurements also show very similar results (μ_{eff} = 1.98 μ_B for **CuL¹** and 2.00 μ_B for **CuL²** and very small Curie–Weiss constants of about –1. The EPR spectra of both complexes show axial symmetry, very similar averaged *g* values of 2.123 and 2.125, respectively, and no hyper-fine splitting.

Keywords: copper(II); 2-bromomethylpyridine; stereoisomers; magnetization; EPR



Citation: Garci, F.; Chebbi, H.; Rouzbeh, N.; Rochels, L.; Disch, S.; Haseloer, A.; Sebastian, S.S.; Ruschewitz, U.; Anthony, E.T.; Klein, A.; et al. Structure, Optical and Magnetic Properties of Two Isomeric 2-Bromomethylpyridine Cu(II) Complexes [Cu(C₆H₉NBr)₂(NO₃)₂] with Very Different Binding Motives. *Molecules* **2023**, *28*, 731. <https://doi.org/10.3390/molecules28020731>

Academic Editor: Athanassios C. Tsipis

Received: 14 December 2022

Revised: 29 December 2022

Accepted: 5 January 2023

Published: 11 January 2023



Copyright: © 2023 by the authors. Licensee MDPI, Basel, Switzerland. This article is an open access article distributed under the terms and conditions of the Creative Commons Attribution (CC BY) license (<https://creativecommons.org/licenses/by/4.0/>).

1. Introduction

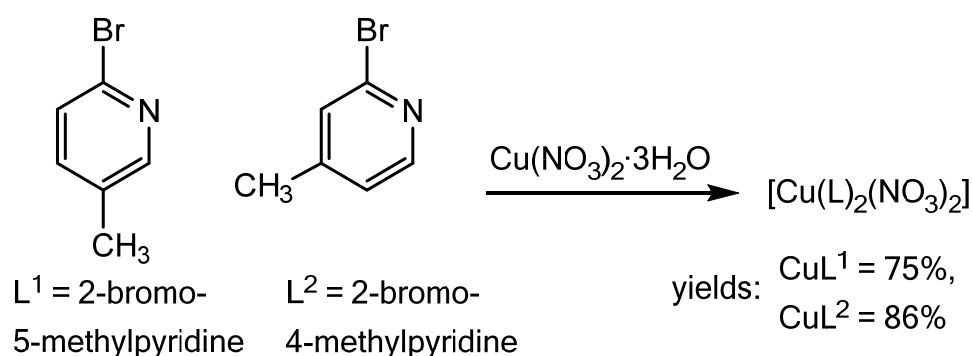
For the development of new interesting materials based on coordination compounds, polytopic or polyfunctional ligands are interesting candidates [1–10]. Both types can help to selectively assemble discrete mononuclear or polynuclear complexes [1–4,7–9], clusters [6,7], or coordination polymers [1–8] including metal-organic frameworks (MOFs) [8,10] either by providing more than one coordination site (polytopic) or other functionalities (polyfunctional) enabling secondary interactions such as hydrogen bonds, halogen bonds, π -stacking, or hydrophobic van der Waals interactions [11–16]. Additionally, the nature of the ligand combined with the *hard* and *soft acids-and bases principle* (HSAB) help in taming the quite

flexible geometries of many 3D transition metals. Thus, using the very simple synthesis approach of mixing ligands and transition metal precursors in solution and precipitating or crystallizing the products, defined materials with interesting catalytic [17–21], electrochemical [21,22], magnetic [23–25], photochemical [26–33], and photophysical properties [30–35] have been obtained in good yields.

Cu(II) is an interesting metal for magnetic materials due to its unpaired spin ($S = \frac{1}{2}$) in its d^9 configuration. The careful design of polyfunctional ligands has allowed to generate dinuclear or oligonuclear Cu(II) coordination compounds with paramagnetic (isolated spins) [24,33], antiferromagnetic (two coupled spins) [23,36], ferromagnetic [37,38], or ferrimagnetic (coupled spins of different species) properties [23,36,39–42].

Within the vast group of polyfunctional ligands, halogenated pyridines are interesting candidates for the formation of supramolecular materials due to their ability to coordinate to metals using the pyridine function and at the same time potentially form intermolecular halogen bonds to aggregate into supramolecular structures in the solid [14,17,40]. However, only a few Cu(II) complexes or coordination polymers with simple halido-pyridines have previously been reported [43–45].

Herein, we report the reaction of $\text{Cu}(\text{NO}_3)_2 \cdot 3\text{H}_2\text{O}$ with 2-bromo-5-methylpyridine and 2-bromo-4-methylpyridine (Scheme 1) forming the two isomeric complexes $[\text{Cu}(\text{L})_2(\text{NO}_3)_2]$. The two compounds show very different structural features (in single crystal X-ray studies and Hirshfeld analyses) which also translate into the optical (UV–vis absorption) and magnetic properties (magnetism and EPR). We also report their FT-IR and Raman characterization and thermal properties.



Scheme 1. Synthesis and yields of the two Cu(II) complexes of this study.

2. Results and Discussion

2.1. Syntheses and Analyses

Reactions of $\text{Cu}(\text{NO}_3)_2 \cdot 3\text{H}_2\text{O}$ with 2-bromo-5-methylpyridine (L^1) in MeCN solution gave the complex $[\text{Cu}(\text{L}^1)_2(\text{NO}_3)_2]$ (**CuL¹**) in 75% yield, while the reaction with 2-bromo-4-methylpyridine (L^2) produced $[\text{Cu}(\text{L}^2)_2(\text{NO}_3)_2]$ (**CuL²**) in 86% yield (Scheme 1, details in the Section 3), both as deep blue crystals. The two stereoisomers showed identical CHN analyses.

2.2. Crystal Structures

The two isomers of the title compound $[\text{Cu}(\text{L})_2(\text{NO}_3)_2]$ ($\text{L}^1 = 2\text{-bromo-5-methylpyridine}$ or $\text{L}^2 = 2\text{-bromo-4-methylpyridine}$) crystallized in two different structures (Figure 1). The 5-methyl isomer **CuL¹** was solved in the monoclinic space group $P2_1/c$ ($Z = 2$) with the cell parameters $a = 6.7738(7)$ Å, $b = 13.1890(9)$ Å, $c = 10.0999(10)$ Å, $\beta = 103.298(8)^\circ$, and a unit cell volume of $878.13(14)$ Å³ (Table S1, Supplementary Materials). The 4-methyl derivative **CuL²** was solved and refined in the triclinic space group $P\bar{1}$ ($Z = 2$) with the cell parameters $a = 7.4916(5)$ Å, $b = 10.0404(7)$ Å, $c = 12.0723(8)$ Å, $\alpha = 86.176(6)^\circ$, $\beta = 77.769(5)^\circ$, $\gamma = 79.793(5)^\circ$, and a unit cell volume of $873.00(10)$ Å³ (Table S1).

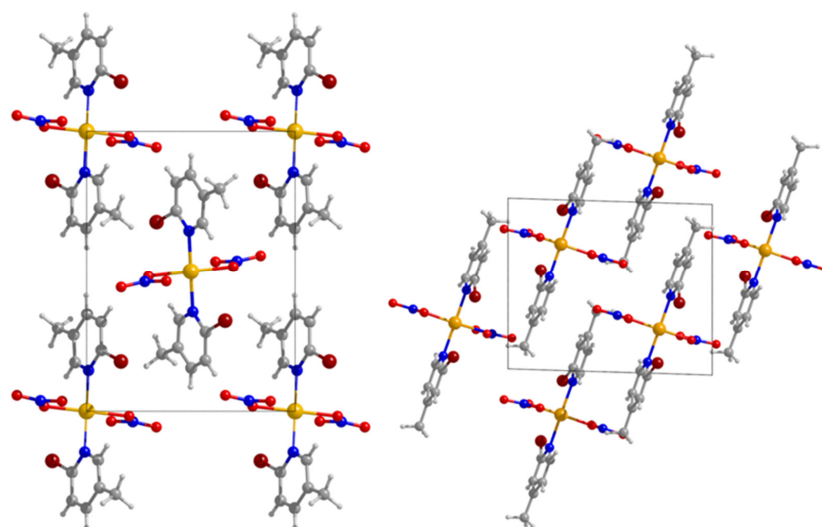


Figure 1. Projection of the crystal structures of $[\text{Cu}(\text{L})_2(\text{NO}_3)_2]$. (left): CuL^1 , L^1 = 2-bromo-5-methylpyridine complex in $P2_1/c$; (right): CuL^2 , L^2 = 2-bromo-4-methylpyridine derivative in $P\bar{1}$, both viewed along the crystallographic a axis. Yellow balls represent Cu atoms, light red = O, blue = N, grey = C, white = H, and dark red = Br atoms.

The molecular entities of both forms show the same coordination pattern around the Cu(II) centers, which is *trans* square planar with two pyridine N atoms and two nitrate O atoms contributing to a square planar N_2O_2 coordination (Figures 2 and 3; essential metrical data in Table S2). For the 2-bromo-5-methylpyridine complex CuL^1 ($P2_1/c$), two additional O atoms from the coordinated NO_3^- ligands O1 and O1' (with $i = -x + 2, -y, -z + 2$) contribute to an overall elongated octahedral ($4 + 2$) coordination with $\text{Cu} \cdots \text{O}_{\text{axial}}$ distances of 2.515(7) Å (Table S2). The Cu–O bonds are much longer than those of the two equatorial O atoms and due to the small bite angle of the NO_3^- ligand, these two O atoms are not in an ideal position for a perfect tetragonally elongated octahedron (D_{4h}). The additional deviation of the two axial ligands distorts the coordination sphere towards an overall C_{2v} symmetry. The tetragonal elongation is frequently found for Cu(II) complexes [46–48], this C_{2v} deviation has been previously observed for derivatives with equatorial-axial chelate ligands [46,47]. The previously reported Cu(II) bis-nitrato bis-pyridine complexes $[\text{Cu}(\text{L})(\text{NO}_3)_2]$ (L = 2-chloro-5-methylpyridine [49] and $[\text{Cu}(4\text{-MTPP})(\text{NO}_3)_2]$ (4-MTPP = 4-(methylthio)-4-(pyridin-2-yl)pyrimidine [50] and the bis-pyridine-N-oxide complex $[\text{Cu}(2,6\text{-dmnpn})_2(\text{NO}_3)_2]$ (2,6-dmnpn = 4- NO_2 -2,6- Me_2 -pyridine-N-oxide) [51] show the same type of bonding with very similar geometry around Cu(II), while $[\text{Cu}(\text{Py})_2(\text{NO}_3)_2]$ Py has a dimeric structure with the Cu-bound O_{NO_3} atom bridging between the Cu(II) centers [52].

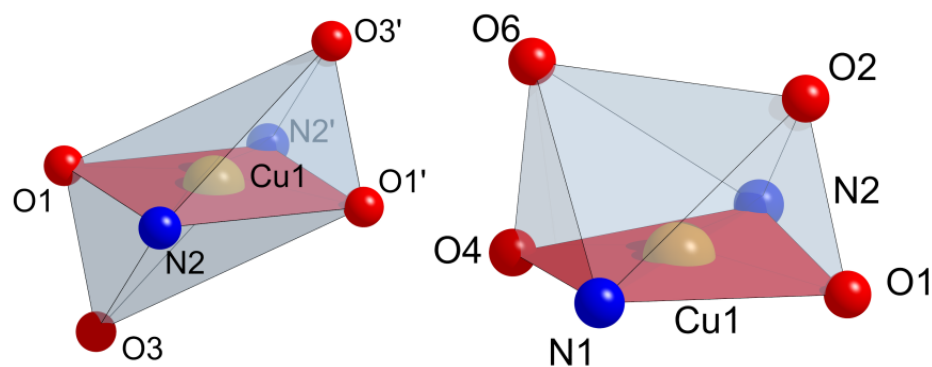


Figure 2. Environment of the Cu atom in the two isomers of $[\text{Cu}(\text{L})_2(\text{NO}_3)_2]$ with atom numbering. (left): CuL^1 , L^1 = 2-bromo-5-methylpyridine in $P2_1/c$; (right): CuL^2 , L^2 = 2-bromo-4-methylpyridine in $P\bar{1}$.

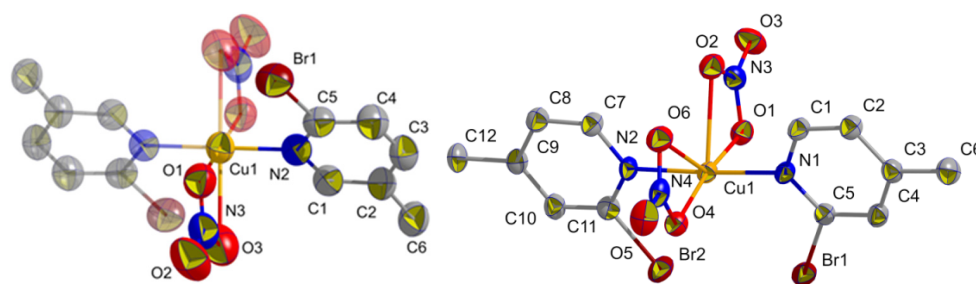


Figure 3. The asymmetric unit of the two isomers of $[\text{Cu}(\text{L})_2(\text{NO}_3)_2]$ with atom numbering. (**left**): CuL^1 , $\text{L}^1 = 2\text{-bromo-5-methylpyridine}$ in $P2_1/c$; (**right**): CuL^2 , $\text{L}^2 = 2\text{-bromo-4-methylpyridine}$ in $P\bar{1}$.

This stands in contrast to the 2-bromo-4-methylpyridine derivative (CuL^2), where two further O atoms of the NO_3^- ligands (O2 and O6) are both localized on the same side of the equatorial N_2O_2 plane. Thus, they form a rather unusual double-tipped square pyramidal coordination around Cu(II). However, whilst this arrangement also agrees with the Jahn–Teller distortion of the Cu(II) d^9 system [47], it is rather exotic. In the case of the 2-bromo-4-methyl ligand, this peculiar orientation of the two NO_3^- ligands is in line with the crystal symmetry (Cu does not lie at the center of the inversion) and goes along with the two Br substituents pointing in the same direction which could be called a *syn* conformation, contrasting with the *anti* conformation of the two Br atoms in the 2-bromo-5-methyl derivative. The $\text{Br} \cdots \text{Br}$ distance of 3.694(3) Å in CuL^2 is slightly shorter than the sum of the van der Waals radii of 3.72 Å [53], while the $\text{Cu} \cdots \text{Br}$ distance of about 3.26 Å is far too long to account for coordination (3.33 Å for CuL^1).

In the crystal structure, both forms show a number of intermolecular hydrogen bonds (Table S3). The shortest ones for CuL^1 with ~2.58 Å are found between O2 and the H–C4 and H–C6 groups of the pyridine ligand, while for CuL^2 slightly shorter intermolecular distances of about 2.39 (O4 \cdots H–C12), 2.48 (O6 \cdots H–C12), and 2.49 Å (O5 \cdots H–C10) were found. All these hydrogen bonds are considered to be weak and essentially of an electrostatic nature [54]. Intermolecular $\text{Br} \cdots \text{Br}$ halogen bonds were not observed, the two Br substituents in CuL^2 point towards H–C3 and H–C6 functions of neighboring molecules with $\text{Br} \cdots \text{H}$ contacts longer than 3 Å (Figure S1).

Powder X-ray diffraction (PXRD) showed an excellent match of the experiment with the patterns calculated from the single crystal XRD for CuL^1 (Figure S2). The powder diffractogram of CuL^2 also matched with the pattern calculated from the single crystal structure but the materials show a lower degree of crystallinity (broader signals) (Figure S3). Nevertheless, the PXRD patterns of both compounds confirm that they are phase-pure and thus suitable for the measurement of thermal, spectroscopic, and magnetic properties.

2.3. Hirshfeld Surface Analysis and Energy Framework Calculations

Hirshfeld surface analysis was carried out for a more detailed view on the intermolecular interactions. The important intermolecular interactions in the molecule are highlighted by the d_i and d_e plotted as fingerprints. The fingerprint plot analysis for CuL^1 showed that intermolecular $\text{H} \cdots \text{O}$ interactions make the highest contribution with 44.6% of the total, while others are markedly smaller 14.6% ($\text{H} \cdots \text{Br}$), 12.5% ($\text{H} \cdots \text{H}$), 12.4% ($\text{C} \cdots \text{H}$), and 5% ($\text{N} \cdots \text{H}$), respectively (Figure S4). For CuL^2 , the $\text{O} \cdots \text{H}$ interactions account for 41.2% which is slightly lower than the 44.6% for the CuL^1 derivative and stands somewhat in contrast to the shorter hydrogen bonds found in the crystal structures for the CuL^2 complex. However, this analysis summarizes the interactions and does not weight them. The $\text{Br} \cdots \text{H}$ (15.9%), $\text{H} \cdots \text{H}$ (13.4%), $\text{C} \cdots \text{H}$ (9.4%), and $\text{N} \cdots \text{H}$ (4.8%) interactions are also very similar.

An energy framework analysis [55] was carried out for the two compounds (Figure S5, Table S4). The interaction energies include electrostatic ($E'_{\text{ele}}(\text{L}^1) = -39.9 \text{ kJ mol}^{-1}$; $E'_{\text{ele}}(\text{L}^2) = -168.6 \text{ kJ mol}^{-1}$), polarization ($E'_{\text{pol}}(\text{L}^1) = -33 \text{ kJ mol}^{-1}$; $E'_{\text{pol}}(\text{L}^2) = -144.1 \text{ kJ mol}^{-1}$), dispersion ($E'_{\text{dis}}(\text{L}^1) = -120.6 \text{ kJ mol}^{-1}$; $E'_{\text{dis}}(\text{L}^2) = -269 \text{ kJ mol}^{-1}$), and repulsion ($E'_{\text{rep}}(\text{L}^1) = 58.9 \text{ kJ mol}^{-1}$; $E'_{\text{rep}}(\text{L}^2) = 157.7 \text{ kJ mol}^{-1}$) contributions with a total interaction energy

of $E_{\text{tot}}(\text{L}^1) = -122.7 \text{ kJ mol}^{-1}$ for **CuL¹** and $E_{\text{tot}}(\text{L}^2) = -340.4 \text{ kJ mol}^{-1}$ for **CuL²**. When comparing the individual contributions, it becomes clear that all of them are higher for **CuL²** (or lower for the repulsion) due to the lower symmetry. However, concerning the resulting marked difference in total energy of $-122.7 \text{ kJ mol}^{-1}$ for **CuL¹** vs. $-340.4 \text{ kJ mol}^{-1}$ for **CuL²**, we are skeptical, because the thermal properties and the IR and Raman spectroscopy of the two complexes are not very different (see later). In future work, we will calculate the stability of the two complexes in the crystal lattice in more detail using density functional theory (DFT) methods.

2.4. Infrared and Raman Spectroscopy

The asymmetric and symmetric H–C vibrations of the CH₃ and CH groups of both complexes were observed in the FT-IR spectra in the range from 3150 to 2850 cm^{−1} followed by aromatic H–C overtones in the 2800–1700 cm^{−1} range (Figure S6) [56–60]. When comparing the two complexes **CuL¹** and **CuL²** (L¹ = 2-bromo-5-methylpyridine, L² = 2-bromo-4-methylpyridine), similar resonances were found in the range from 1600 to 120 cm^{−1} (Figure 4). The underlying pyridine C=C and C=N and NO₃ stretching frequencies were generally at a higher energy for the **CuL¹** complex and the relative intensities differ between the two stereoisomers with their different coordination pattern. The same is true for the umbrella-like H–C vibration modes of the CH₃ substituents, the H–C arene oscillations, the H–C wagging, and the C–Br stretches [56–58] in the range from 1150 to 900 cm^{−1}. Even more different are the Raman spectra of the two complexes (Figure S7). However, here all the characteristic bands are shifted to a lower energy for the **CuL¹** complex compared with the **CuL²** derivative especially the C–Br stretches at around 800 cm^{−1} and the NO₃ stretches at around 700 cm^{−1} which are also found in the FT-IR. Additionally, the Cu–N and Cu–O stretches in the range between 400 and 200 cm^{−1} are shifted to lower energy for the **CuL¹** derivative which would mean slightly weaker Cu–ligand bonds. However, the thermal analyses (TG/DTA) do not show marked differences in their behavior (see below) and the different *T* of the single crystal X-ray diffraction data precludes comparison.

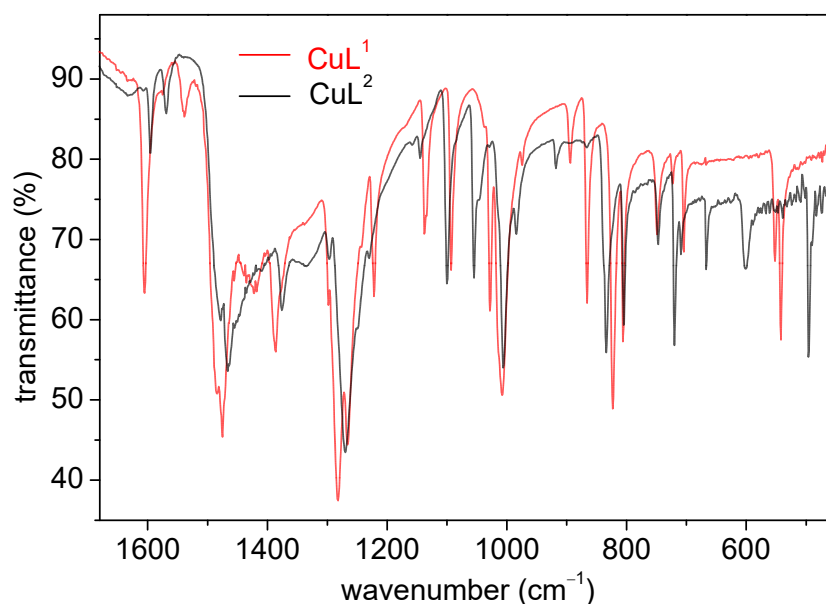


Figure 4. FT-IR spectra of the complexes **CuL¹** (L¹ = 2-bromo-5-methylpyridine) (red) and **CuL²** (L² = 2-bromo-4-methylpyridine) (black).

2.5. Thermal Analysis

Thermogravimetric (TG) analyses shows that the two compounds are thermally stable up to about 160 °C (Figure S8). The differential thermal analysis (DTA) shows an endothermic peak at around 200 °C for both complexes (slightly higher for **CuL²**), followed by one or two intense exothermic signals in the range 220 to 300 °C. We assume the decomposition

of the nitrate ligands to NO, NO₂, and O₂ being responsible for these exothermic peaks. The final mass loss after heating to 300 °C is 83% for **CuL**¹ and 86% for **CuL**², which is in line with the formation of CuO (calculated loss of 85%). The same behavior was observed for comparable Cu(II) complexes [60–63].

2.6. UV–Vis Absorption Spectroscopy

The two complexes show very similar absorption spectra in EtOH solution. An intense band around the 220 nm is identical for both complexes (Figure 5). Marked differences were found in the UV–vis range where the **CuL**¹ complex shows a maximum at 270 nm, while the same band for the **CuL**² derivative is found at 263 nm. These bands can be assigned to π – π^* transition as they also occur for the ligands (Figure S9). For the **CuL**¹ complex, we observed a broad shoulder in the range from 300 to 350 nm which we assign to a ligand(NO₃)[−]-to-metal-charge transfer excitation. For the **CuL**² derivative, this is far less pronounced which we ascribe to the unusual orientation of the two NO₃[−] ligands compared to **CuL**¹. The long-wavelength absorptions at around 750 nm are quite similar for both complexes (743 nm for **CuL**¹, 753 nm for **CuL**²). They were assigned to the $^2B_{2g} \rightarrow ^2E_g$ and $^2A_{1g} \rightarrow ^2E_g$ electronic transitions in Cu(II), d⁹ systems [29,32,46,59,63]. They are responsible for the typical blue color of the two Cu(II) complexes.

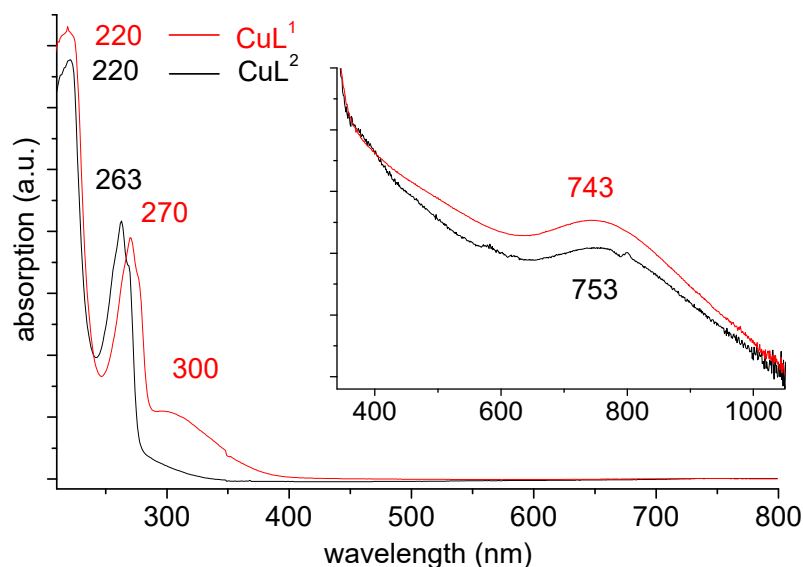


Figure 5. UV–vis absorption spectra of the complexes **CuL**¹ (**L**¹ = 2-bromo-5-methylpyridine and **CuL**², **L**² = 2-bromo-4-methylpyridine, in EtOH solution. Conc. for the main spectra = 10^{−4} mol/L; conc. for the insert = 10^{−3} mol/L).

While the similar NIR bands might point to a decomposition of the complexes in EtOH solution, forming the non-coordinated ligands and a [Cu(II)(EtOH)_n]²⁺ solvate, the bands in the 300–350 nm range which do not occur for the ligands, support that the complexes were stable in EtOH solution. If that is the case, we conclude that the NIR absorptions of the complexes are either not affected by the different coordination of the two isomers, or **CuL**² forms the same *anti* structure as **CuL**¹ in solution. In future work, we will study this possibility in more detail.

2.7. Magnetization and EPR Studies

Temperature-dependent magnetic susceptibility data (Figure 6) reveal a nearly perfect paramagnetic behavior in the entire temperature range from 5 to 350 K, in line with the isolated Cu(II) centers. A Curie–Weiss fit of the inverse magnetic susceptibility yields nearly identical effective magnetic moments of $\mu_{\text{eff}} = 1.98 \mu_B$ for **CuL**¹ and $\mu_{\text{eff}} = 2.00 \mu_B$ for **CuL**². Both are constant over a wide temperature range and within the range from 1.7 to 2.2 μ_B

experimentally observed for similar Cu(II) complexes at room temperature [25,64–70]. The effective moments being larger than the spin-only value of $1.73 \mu_B$ expected for a $3d^9$ configuration ($S = 1/2$) indicate spin-orbit coupling [23,37,39,64,65].

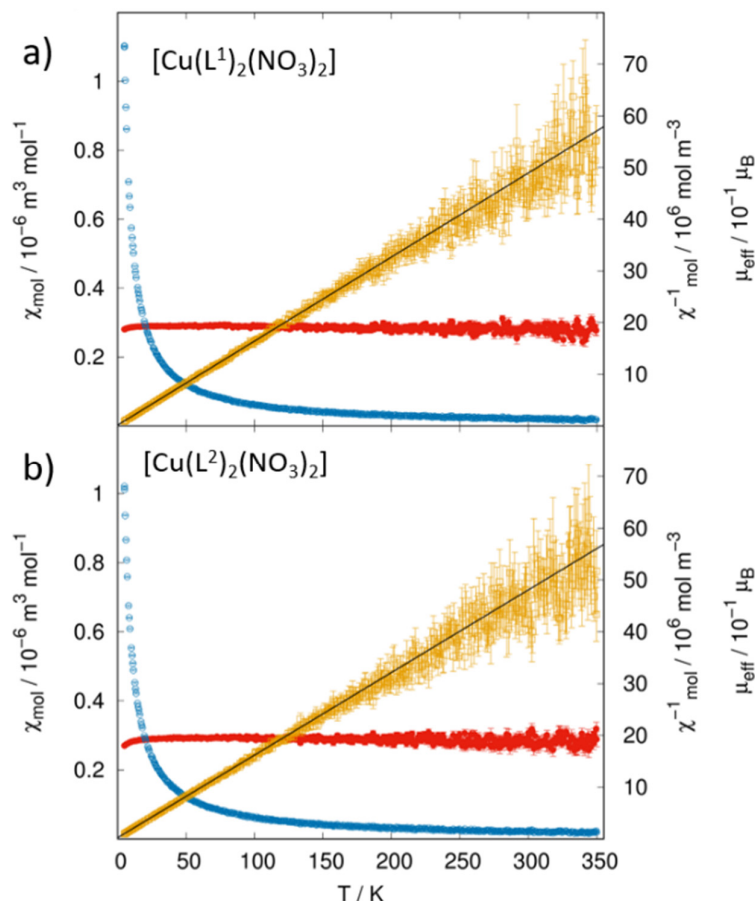


Figure 6. Molar susceptibilities (blue circles) and inverse molar susceptibilities (orange squares) of (a) **CuL¹** and (b) **CuL²** with fits according to the Curie–Weiss law (black solid line). The red curve represents the effective magnetic moments (in μ_B).

Based on $S = 1/2$ we calculated g values of 2.29 for **CuL¹** and 2.32 for **CuL²** from the magnetic moments. The azido-bridged coordination polymers $[\text{Cu}(\text{4-HOCH}_2\text{py})(\mu_{1,1}\text{-N}_3)(\mu_{1,3}\text{-N}_3)]_n$ and $[\text{Cu}(\text{2-Br-4-Mepy})(\mu^{1,1}\text{-N}_3)_2]_n$ with five-coordinated Cu(II) showed a similar T -independent behavior as **CuL¹** and **CuL²** and their g values of 2.22 and 2.09, respectively, are also in the same range. The authors assign this to antiferromagnetic coupling through the bridging azide ligands [68]. For the mononuclear complex $[\text{Cu}(\text{L})_2\text{Cl}_2]$ (L = pyridine-4-carboxamido-2-methyl-phenyl-4-methyl ester) with a square planar Cu(II) a smaller g value of 2.13 was reported [69], while for the mononuclear pyridine- N -oxide complex $[\text{Cu}(\text{C}_5\text{H}_5\text{NO})_2(\text{NO}_3)_2]$ with a similar coordination as **CuL¹** and **CuL²** a g value of 2.17 was reported [66].

The Weiss constants of -1 K (**CuL¹**) and -1.5 K (**CuL²**) are comparably small. A Weiss constant >0 indicates dominating ferromagnetic interactions and for <0 dominating antiferromagnetic interactions [23,64]. Thus, we can attribute a weak antiferromagnetic character to both complexes. For the pyridine- N -oxide Cu(II) complex $[\text{Cu}(\text{C}_5\text{H}_5\text{NO})_2(\text{NO}_3)_2]$ a very similar Weiss constant of -0.8 K was reported [66] and the values for the azido-bridged coordination polymers $[\text{Cu}(\text{4-HOCH}_2\text{py})(\mu_{1,1}\text{-N}_3)(\mu_{1,3}\text{-N}_3)]_n$ (-1.3 K) and $[\text{Cu}(\text{2-Br-4-Mepy})(\mu^{1,1}\text{-N}_3)_2]_n$ (-1.1 K) are only slightly smaller [68] in line with their small antiferromagnetic coupling. The similar T -independent behavior (see above) and the very similar Weiss constants for **CuL¹**, **CuL²**, and these azido-bridged complexes is interesting as in the

azido-bridged complexes the antiferromagnetic coupling is promoted through the bridging azido ligands, while in **CuL¹** and **CuL²**, no such direct interactions between the Cu(II) centers occur. In contrast to this, a Weiss constant of -9.31 K was reported for the tetrachlorido cuprate(II) $[\text{Cu}(\text{bix})\text{Cl}_4] \cdot \text{H}_2\text{O}$ ($\text{bix} = 1,4\text{-bis}(\text{imidazol-1-ylmethyl})\text{benzene}$) [67] which is likely due to strong $\text{O-H} \cdots \text{Cl}$ hydrogen bonds connecting the tetrahedral $[\text{CuCl}_4]^{2-}$ units in the structure. Thus, both g values and the Weiss constants from magnetic measurements do not allow unequivocal conclusions on the structures of Cu(II) complexes.

The X-band EPR spectra of a powder sample of **CuL¹** showed an axial spectrum (Figure 7) with no hyperfine splitting (HFS). The spectrum was simulated (Figure S10) using the g values $g_{\parallel} = 2.230$ and $g_{\perp} = 2.070$, which average to $g_{\text{av}} = 2.123$, the g anisotropy Δg calculates to 0.160 (Table 1).

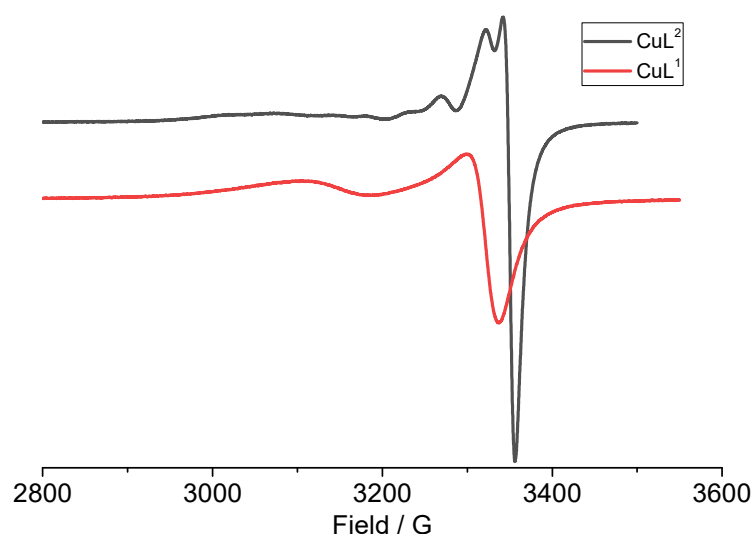


Figure 7. X-band EPR spectra of the two Cu(II) complexes $[\text{Cu}(\text{L})_2(\text{NO}_3)_2]$, recorded on solid samples at frequencies of 9.642502 GHz for **CuL²** ($\text{L}^2 = 2\text{-bromo-4-methylpyridine}$) and 9.645555 GHz for **CuL¹** ($\text{L}^1 = 2\text{-bromo-5-methylpyridine}$) at 298 K. Receiver gain of 40, attenuation 25 dB (0.3162 mW), 1 scan for both samples.

Table 1. X-band EPR data of the two complexes $[\text{Cu}(\text{L})_2(\text{NO}_3)_2]^a$.

	g_{\parallel}	g_{\perp}	g_{av}	Δg	HFS ^b	Line Width ^c
$[\text{Cu}(\text{L}^1)_2(\text{NO}_3)_2]$	2.230	2.070	2.123	0.160	none	50, 27, 27
$[\text{Cu}(\text{L}^2)_2(\text{NO}_3)_2]$ species I	2.260	2.057	2.125	0.203	none	95, 22, 22
species II	2.135	2.057	2.083	0.078	$A_{\parallel\text{N}/\text{Cu}} = 40$ G	15, 10, 10

^a Powdered samples at 298 K, $\text{L}^1 = 2\text{-bromo-5-methylpyridine}$, $\text{L}^2 = 2\text{-bromo-4-methylpyridine}$. Averaged g value $g_{\text{av}} = (g_{\parallel} + 2g_{\perp})/3$; g anisotropy $\Delta g = g_{\parallel} - g_{\perp}$. ^b Hyperfine splitting (HFS) in G. ^c Simulated line width in G.

In contrast to this, we observed two signals for **CuL²** ($\text{L}^2 = 2\text{-bromo-4-methylpyridine}$) (Figure 7; Figure S11). Simulations allowed to identify one species with similar parameters as the **CuL¹** complex, $g_{\parallel} = 2.260$ and $g_{\perp} = 2.057$, which averages to $g_{\text{av}} = 2.125$. The g anisotropy Δg for this species calculates to 0.203 (species I in Table 1). We conclude that this spectrum represents **CuL²**, which is supported by the missing HFS in both spectra. The spectrum of the second species was simulated using $g_{\parallel} = 2.135$ and $g_{\perp} = 2.057$, which averages to $g_{\text{av}} = 2.083$. The g anisotropy Δg calculates to 0.078 (species II in Table 1). Here, pronounced HFS of $^{63/65}\text{Cu}$ ($I = 3/2$) and ^{14}N ($I = 1$) was observed. At the moment, we have no idea about the nature of the second Cu(II) species and how the PXRD failed to detect it in the **CuL²** product. It may be that the EPR sample of **CuL²** contained molecules of both *syn* and *anti* conformations in the same crystal structure. Such *syn*-to-*anti* conversion was already discussed for the UV-vis absorption spectroscopy in solution. To observe this in the solid would be even more fascinating and we will study this in detail in the near future.

The g values derived from the magnetic measurements of 2.29 for **CuL¹** and 2.32 for **CuL²** both lie higher than the averaged g values from EPR spectroscopy but both values are higher for **CuL²** while the values from the magnetic measurements roughly coincide with the g_{\parallel} values from EPR. We attribute these differences to the specific geometry and orientation of crystallites in the EPR experiment.

For the geometrically very similar complex $[\text{Cu}(\text{2,6-dmnpn})_2(\text{NO}_3)_2]$ (2,6-dmnpn = 4-NO₂-2,6-Me₂-pyridine-N-oxide) [51], three g values $g_z = 2.295$, $g_y = 2.086$, $g_x = 2.066$ were reported. Overall, the spectrum looked very similar to those of **CuL¹** and **CuL²** with a slightly different $g_{\text{av}} = 2.149$ which is probably due to the O–Cu bonding of the pyridine-N-oxide ligands, but a $\Delta g = 0.229$ which is very similar to our values. We have recently shown that EPR spectra of such pseudo-axial geometry (g_y and g_x very similar) are frequently observed for Cu(II) complexes containing pyridine-amide ligands. Very similar g_{av} values of over 2.1, Δg values of around 0.2 and no HFS are in line with various tetragonally elongated octahedral structures [46]. Although the local symmetry around Cu(II) is very different for **CuL¹** and **CuL²**, EPR spectroscopy does not allow for tracing of the two very different distortion variants from the ideal octahedral geometry.

3. Experimental Section

3.1. Chemicals

$\text{Cu}(\text{NO}_3)_2 \cdot 3\text{H}_2\text{O}$ was purchased from Fluka (Fisher Scientific, Schwerte, Germany), 2-bromo-5-methylpyridine and 2-bromo-4-methylpyridine were purchased from BLDpharm (BLDpharm, Kaiserslautern, Germany) and used without further purification.

3.2. Syntheses

3.2.1. Synthesis of $[\text{Cu}(\text{L}^1)_2(\text{NO}_3)_2]$ **L¹** = 2-Bromo-5-methylpyridine

A total of 0.241 g (1 mmol) of $\text{Cu}(\text{NO}_3)_2 \cdot 3\text{H}_2\text{O}$ was dissolved in 3 mL of MeCN and added to 3 mL of MeCN solution containing 0.170 g (1 mmol) 2-bromo-5-methylpyridine. The mixture was stirred for 3 h and then a blue solution was filtered from a blue solid residue. From the blue solution, crystals were obtained through slow evaporation at ambient conditions. Yield: 403 mg (0.75 mmol, 75%) of blue crystals. Elemental analysis ($\text{C}_{12}\text{H}_{12}\text{Br}_2\text{CuN}_4\text{O}_6$): calcd. (found), C 27.11 (27.10), H 2.28 (2.25), N 10.54 (10.55)%. FT-IR: 3095, 3026, 1596, 1380, 1478, 1277, 995, 830, 750, 494 cm^{-1} . UV–vis (in EtOH): 220, 270, 300sh, 743 nm.

3.2.2. Synthesis of $[\text{Cu}(\text{L}^2)_2(\text{NO}_3)_2]$ **L²** = 2-Bromo-4-methylpyridine

A total of 0.126 g (0.52 mmol) of $\text{Cu}(\text{NO}_3)_2 \cdot 3\text{H}_2\text{O}$ was dissolved in 2 mL of EtOH and added to 2 mL of EtOH solution containing 90 mg (0.52 mmol) of 2-bromo-4-methylpyridine. The mixture was stirred for 3 h and left for evaporation at ambient temperature. Yield: 460 mg (0.86 mmol, 86%) of blue crystals. Elemental analysis ($\text{C}_{12}\text{H}_{12}\text{Br}_2\text{CuN}_4\text{O}_6$): calcd. (found), C 27.11 (27.09), H 2.28 (2.30), N 10.54 (10.51)%. FT-IR: 3110, 3076, 1606, 1455, 1387, 1280, 1003, 830, 703, 534 cm^{-1} . UV–vis (in EtOH): 220, 263 nm, 753 nm.

3.3. Instrumentation

Elemental analyses were carried out using a Hekatech CHNS EuroEA 3000 Analyzer (Hekatech, Wegberg, Germany). Raman measurement was carried out using the Renishaw inVia Reflex Raman (Renishaw, Kingswood, UK). TG measurements were performed using a simultaneous Mettler Toledo TGA/DSC 2/1600 thermal analyzer (Mettler Toledo, Barcelona, Spain) in an N₂ atmosphere at a heating rate of 10 K min^{−1}. Fourier-transformed infrared (FT-IR) spectra on KBr pellets were obtained using a PerkinElmer UATR II spectrometer (Perkin Elmer, Waltham, MA, USA) in the range from 4000 to 400 cm^{-1} at room temperature. UV–vis absorption spectra were recorded in EtOH using a SCINCO S-3100 spectrophotometer (Scinco, Seoul, Republic of Korea) or a Varian Cary 05E spectrophotometer (Varian, Darmstadt, Germany). EPR spectroscopy was measured on solid samples

in the X-band using a Bruker EMXNano spectrometer (Bruker, Rheinhausen, Germany) at 298 K; g values were calibrated using dp_{pph}.

3.4. Magnetization Measurements

The magnetic properties were studied using a Quantum Design PPMS Evercool II (Quantum Design GmbH, Darmstadt, Germany) with vibrating sample magnetometer (VSM) option. Then, 12.8 mg of **CuL¹** and 10.1 mg of **CuL²** of powdered samples were enclosed in commercially available polypropylene powder capsules and fixed in a brass sample holder. The temperature-dependent magnetization was measured after cooling in an applied field of 10 mT in a temperature range from 5 to 350 K with a heating rate of 1 K min^{−1}. A small background signal resulting from the sample holder was determined from reference measurements and subtracted from the measured sample data. The obtained susceptibility data were corrected for a diamagnetic susceptibility of $\chi_{\text{dia}} = -271.88 \times 10^{-11} \text{ m}^3 \text{ mol}^{-1}$ [64]. A fit of the inverse molar susceptibility data according to the Curie–Weiss law was carried out in the temperature range from 20 to 220 K.

3.5. Single-Crystal X-ray Diffraction

The x-ray single crystals structure analyses were carried out at 293(2) K for **[Cu(L¹)₂(NO₃)₂]** and at 150(2) K for **[Cu(L²)₂(NO₃)₂]** with a Stoe IPDS 2T diffractometer and equipped with graphite-monochromatized Mo-K α radiation. The structures were solved by using SHELXT2018/3 [71] and refined using SHELXL [72,73]. A summary of the crystal data, experimental details, and refinement results are provided in Table S1. CCDC 2207776 for **[Cu(L¹)₂(NO₃)₂]** (L¹ = 2-bromo-5-methylpyridine) and 2207769 for **[Cu(L²)₂(NO₃)₂]** (L² = 2-bromo-4-methylpyridine) contain the supplementary crystallographic data for this paper. These data can be obtained free of charge at www.ccdc.cam.ac.uk/conts/retrieving.html (accessed on 4 December 2022) or from the Cambridge Crystallographic Data Centre, Cambridge, 12 Union Road, Cambridge, CB2 1EZ UK. Fax: +44-1223-336-033; Email: deposit@ccdc.cam.ac.uk.

3.6. Powder X-ray Diffraction

PXRD data were collected at room temperature on a Rigaku MiniFlex 600-C powder diffractometer, Cu K α radiation ($\lambda = 1.54186 \text{ \AA}$, Ni filter, 293(2) K, $3^\circ \leq 2\theta \leq 90^\circ$), D/teX Ultra silicon strip detector. Typical recording times were approx. 20 min with a step size of 0.005° (2θ). Employing the WinXPow software suite (WinXpow, version 3.12, Stoe & Cie GmbH, Darmstadt, Germany) the recorded patterns were compared with theoretical patterns simulated from known single-crystal structure data.

3.7. Hirshfeld Surface Analysis

Hirshfeld surface analysis, their relative 2D fingerprint plots, and the energy framework calculations are an essential technique for showing packing modes and intermolecular interactions of crystals' structure using a CIF file in the Crystal Explorer 17 software [74]. The quantifying and decoding of the inter molecular contacts in the crystal packing are visualized using d_{norm} (normalized contact distance) and 2D fingerprint plots, respectively. The dark-red spots on the d_{norm} surface arise as a result of short interatomic contacts, while the other inter molecular interactions appear as light-red spots. d_i (inside) and d_e (outside) represent the distances to the Hirshfeld surface from the nuclei, with respect to the relative van der Waals radii. The proportional contribution of the contacts over the surface is visualized by the color gradient (blue to red) in the fingerprint plots. The energy framework calculations are estimated from a single point molecular wave function at HF/3-21G. A cluster of 3.8 \AA radius was generated around the molecule and the energy calculation was performed. The neighboring molecules (density matrices) are generated within this shell by applying crystallographic symmetry operations with respect to the central molecule (density matrix). The interaction energy is broken down as $E_{\text{tot}} = k_{\text{ele}}E'_{\text{ele}} + k_{\text{pol}}E'_{\text{pol}} + k_{\text{dis}}E'_{\text{dis}} + k_{\text{rep}}E'_{\text{rep}}$ where the k values are scale factors, E'_{ele} represents the

electrostatic component, E'_{pol} the polarization energy, E'_{dis} the dispersion energy, and E'_{rep} the exchange–repulsion energy [55,75,76].

4. Conclusions

Reacting $\text{Cu}(\text{NO}_3)_2 \cdot 3\text{H}_2\text{O}$ with the two isomeric 2-bromo-5-methylpyridine (L^1) and 2-bromo-4-methylpyridine (L^2) ligands led to two isomeric 2-bromomethylpyridine $\text{Cu}(\text{II})$ complexes $[\text{Cu}(\text{C}_6\text{H}_9\text{NBr})_2(\text{NO}_3)_2]$ as air-stable blue materials in good yields. The x-ray single crystal diffraction showed different crystal structures $[\text{Cu}(\text{L}^1)_2(\text{NO}_3)_2]$ (CuL^1) in $P2_1/c$, $[\text{Cu}(\text{L}^2)_2(\text{NO}_3)_2]$ (CuL^2) in $P\bar{1}$. The molecular structure showed a primary *trans*- $\text{N}_2(\text{Py})\text{O}_2(\text{NO}_3)$ coordination of the $\text{Cu}(\text{II})$ centers for both complexes but a very different orientation of the Br substituents. The expected structure, which we described as *anti* was found for CuL^1 while CuL^2 , showed an unusual *syn* conformation with neighboring Br atoms and rather short $\text{Br} \cdots \text{Br}$ contacts of about 3.7 Å. Moreover, CuL^1 showed the expected 4+2 distorted coordination with the two secondary (axially elongated) Cu–O bonds from the NO_3 ligands on each side of the CuN_2O_2 basal plane, while for CuL^2 both secondary O atoms lie on the side which is not occupied by the Br substituents. While the general Hirshfeld surface analysis gave very similar results for both structures, an energy framework analysis gave superior stability for CuL^2 due to the lower symmetry. In contrast to this, the thermal stability (TG/DTA) of both complexes is almost the same with decomposition starting at around 160 °C. The FT-IR and Raman frequencies are markedly different for the two isomers. The T -dependent susceptibilities again show very similar results ($\mu_{\text{eff}} = 1.98 \mu_{\text{B}}$ for CuL^1 and $2.00 \mu_{\text{B}}$ for CuL^2 and very small Curie–Weiss constants of about -1 K. The EPR spectra of both complexes show axial symmetry, very similar averaged g values of 2.123 and 2.125, respectively, and no hyper-fine splitting. The only difference here lies in the markedly higher g anisotropy Δg of 0.203 for CuL^2 compared with 0.160 for CuL^1 . In the fluid EtOH solution, the two complexes seem to be stable and UV–vis absorption spectra show marked differences in the π – π^* absorptions at 263 for CuL^2 and 270 for CuL^1 nm and in the ligand-to-metal charge transfer bands at around 320 nm which are pronounced for CuL^1 but very weak for CuL^2 . We assign this difference to the higher symmetry at the $\text{Cu}(\text{II})$ center for CuL^1 . In contrast to this, the long-wavelength d–d* bands at around 750 nm are very similar for both complexes. At the same time, we cannot rule out that CuL^2 is present in solution in the same isomeric *anti* form as CuL^1 and that only lattice energies are responsible for the unexpected structure of CuL^2 in the solid. In future work, we will gauge the stability of the two isomeric forms by sophisticated DFT calculations as well as by UV–vis absorption and EPR spectroscopy.

Supplementary Materials: The following supporting information can be downloaded at: <https://www.mdpi.com/article/10.3390/molecules28020731/s1>, Figure S1: Views on the crystal structure of $[\text{Cu}(\text{L}^2)_2(\text{NO}_3)_2]$ $\text{L}^2 = 2\text{-bromo-4-methylpyridine}$ along the crystallographic c and b axes; Figure S2: X-ray powder diffractogram of $[\text{Cu}(\text{L}^1)_2(\text{NO}_3)_2]$ $\text{L}^1 = 2\text{-bromo-5-methylpyridine}$ measured with $\text{Cu-K}\alpha$ radiation in reflection geometry with the calculated pattern for the corresponding single crystal structure; Figure S3: X-ray powder diffractogram of $[\text{Cu}(\text{L}^2)_2(\text{NO}_3)_2]$ $\text{L}^2 = 2\text{-bromo-4-methylpyridine}$ measured with $\text{Cu-K}\alpha$ radiation in reflection geometry with the calculated pattern for the corresponding single crystal structure; Figure S4: View of the Hirshfeld surfaces mapped over d_{norm} and Hirshfeld two-dimensional fingerprint plots for $[\text{Cu}(\text{L}^1)_2(\text{NO}_3)_2]$ and $[\text{Cu}(\text{L}^2)_2(\text{NO}_3)_2]$; Figure S5: Energy frameworks constructed for Coulomb energy, dispersion energy and total energy for the both compounds $[\text{Cu}(\text{L}^1)_2(\text{NO}_3)_2]$ $\text{L}^1 = 2\text{-bromo-5-methylpyridine}$ in $P2_1/c$ and $[\text{Cu}(\text{L}^2)_2(\text{NO}_3)_2]$ $\text{L}^2 = 2\text{-bromo-4-methylpyridine}$ in $P\bar{1}$; Figure S6: FT-IR spectra of the complexes $[\text{Cu}(\text{L}^1)_2(\text{NO}_3)_2]$ $\text{L}^1 = 2\text{-bromo-5-methylpyridine}$ in $P2_1/c$ and $[\text{Cu}(\text{L}^2)_2(\text{NO}_3)_2]$ $\text{L}^2 = 2\text{-bromo-4-methylpyridine}$ in $P\bar{1}$; Figure S7: Raman spectra of the complexes $[\text{Cu}(\text{L}^1)_2(\text{NO}_3)_2]$ $\text{L}^1 = 2\text{-bromo-5-methylpyridine}$ in $P2_1/c$ and $[\text{Cu}(\text{L}^2)_2(\text{NO}_3)_2]$ $\text{L}^2 = 2\text{-bromo-4-methylpyridine}$ in $P\bar{1}$; Figure S8: TG-DTA curves of $[\text{Cu}(\text{L}^1)_2(\text{NO}_3)_2]$ and $[\text{Cu}(\text{L}^2)_2(\text{NO}_3)_2]$; Figure S9: UV–vis absorption spectra of the ligands $\text{L}^1 = 2\text{-bromo-5-methylpyridine}$ and $\text{L}^2 = 2\text{-bromo-4-methylpyridine}$ in EtOH; Figure S10: X-band EPR spectrum of $[\text{Cu}(\text{L}^1)_2(\text{NO}_3)_2]$, ($\text{L}^1 = 2\text{-bromo-5-methylpyridine}$) at 9.645555 GHz and 298 K with simulation; Figure S11: X-band EPR spectrum of $[\text{Cu}(\text{L}^2)_2(\text{NO}_3)_2]$, ($\text{L}^2 = 2\text{-bromo-4-methylpyridine}$)

at 9.642502 GHz and 298 K with simulation; Table S1: Structure solution and refinement data for the two isomeric forms of $[\text{Cu}(\text{L})_2(\text{NO}_3)_2]$; Table S2: Selected metrical data of the isomeric forms of $[\text{Cu}(\text{L})_2(\text{NO}_3)_2]$; Table S3: Hydrogen bond details of the isomeric forms of $[\text{Cu}(\text{L})_2(\text{NO}_3)_2]$; Table S4: Interaction energies (kJ/mol) of the molecular pairs calculated from energy framework calculation of $[\text{Cu}(\text{L}^1)_2(\text{NO}_3)_2]$ and $[\text{Cu}(\text{L}^2)_2(\text{NO}_3)_2]$.

Author Contributions: Conceptualization: H.C., M.F.Z. and A.K.; methodology: F.G., H.C., A.K. and S.D.; investigation: F.G., A.H., S.S.S., N.R., L.R. and E.T.A.; resources: H.C., M.F.Z., U.R., A.K. and S.D.; data curation: F.G., A.H., N.R., L.R., S.D., A.K., S.S.S. and E.T.A.; visualization: F.G., A.K., S.S.S., S.D. and E.T.A.; supervision and project administration: H.C., U.R. and A.K.; manuscript original draft: F.G. and A.K.; manuscript editing: U.R., S.D., S.S.S. and A.K. All authors have read and agreed to the published version of the manuscript.

Funding: This study was funded by the Tunisian Ministry of Higher Education and Scientific Research. N.R., L.R. and S.D. acknowledge funding by the Deutsche Forschungsgemeinschaft (DFG) DI 1788/2-1.

Institutional Review Board Statement: Not applicable.

Informed Consent Statement: Not applicable.

Data Availability Statement: Available from the authors on request.

Acknowledgments: The authors thank Albert Figuerola, Laboratory of Nanostructured and Nanocomposite Materials (LM2N), Department of Inorganic Chemistry, University of Barcelona, Spain, for differential thermal analysis (DTA) and thermogravimetric (TG) measurements. The XRD platform of the Department of Chemistry, University of Cologne, Germany, is acknowledged for the single crystal XRD measurements. We also thank Olav Schiemann, University of Bonn, Germany, for the EPR facilities and Hamed Alaei, University of Bonn, Germany, for assistance in the EPR measurements. Leo Payen, Department of Chemistry, University of Cologne, Germany, is acknowledged for assistance in the powder XRD measurements.

Conflicts of Interest: The authors declare that they have no conflict of interest.

Compliance with Ethical Standards: The work and report are in full agreement with ethical standards of both universities and national funding agencies, the Deutsche Forschungsgemeinschaft (DFG), and the Tunisian Ministry of Higher Education and Scientific Research.

References

1. D’Vries, R.F.; Gomez, G.E.; Ellena, J. Highlighting Recent Crystalline Engineering Aspects of Luminescent Coordination Polymers Based on F-Elements and Ditopic Aliphatic Ligands. *Molecules* **2022**, *27*, 3830. [\[CrossRef\]](#) [\[PubMed\]](#)
2. Ashbridge, Z.; Fielden, S.D.P.; Leigh, D.A.; Pirvu, L.; Schaufelberger, F.; Zhang, L. Knotting matters: Orderly molecular entanglements. *Chem. Soc. Rev.* **2022**, *51*, 7779–7809. [\[CrossRef\]](#) [\[PubMed\]](#)
3. Housecroft, C.E.; Constable, E.C. The terpyridine isomer game: From chelate to coordination network building block. *Chem. Commun.* **2020**, *56*, 10786–10794. [\[CrossRef\]](#) [\[PubMed\]](#)
4. Yang, Q.; Tang, J. Heterometallic grids: Synthetic strategies and recent advances. *Dalton Trans.* **2019**, *48*, 769–778. [\[CrossRef\]](#) [\[PubMed\]](#)
5. Fugu, M.B.; Ellaby, R.J.; O’Connor, H.M.; Pitak, M.B.; Klooster, W.; Horton, P.N.; Coles, S.J.; Al-Mashhadani, M.H.; Perepichka, I.F.; Brechin, E.K.; et al. Mono- and ditopic hydroxamate ligands towards discrete and extended network architectures. *Dalton Trans.* **2019**, *48*, 10180–10190. [\[CrossRef\]](#)
6. Shiga, T.; Newton, G.N.; Oshio, H. Pre-programmed self-assembly of polynuclear clusters. *Dalton Trans.* **2018**, *47*, 7384–7394. [\[CrossRef\]](#)
7. Ahmad, N.R.; Chughtai, A.H.; Younus, H.A.; Verpoort, F. Discrete metal-carboxylate self-assembled cages: Design, synthesis and applications. *Coord. Chem. Rev.* **2014**, *280*, 1–27. [\[CrossRef\]](#)
8. Cook, T.R.; Zheng, Y.-R.; Stang, P.J. Metal-Organic Frameworks and Self-Assembled Supramolecular Coordination Complexes: Comparing and Contrasting the Design, Synthesis, and Functionality of Metal-Organic Materials. *Chem. Rev.* **2013**, *113*, 734–777. [\[CrossRef\]](#)
9. Dawe, L.N.; Shuvaev, K.V.; Thompson, L.K. Polytopic ligand directed self-assembly—Polymetallic $[n \times n]$ grids versus non-grid oligomers. *Chem. Soc. Rev.* **2009**, *38*, 2334–2359. [\[CrossRef\]](#)
10. Guillermin, V.; Eddaoudi, M. The Importance of Highly Connected Building Units in Reticular Chemistry: Thoughtful Design of Metal-Organic Frameworks. *Acc. Chem. Res.* **2021**, *54*, 3298–3312. [\[CrossRef\]](#)

11. Fernández-Figueiras, A.; Ravutsov, M.A.; Simeonov, S.P. Site-Selective C–H Functionalization of Arenes Enabled by Noncovalent Interactions. *ACS Omega* **2022**, *8*, 6439–6448. [[CrossRef](#)]
12. Lohith, T.N.; Hema, M.K.; Karthik, C.S.; Sandeep, S.; Mallesha, L.; Mallu, P.; Ramalingam, R.J.; Sridhar, M.A.; Karnan, M.; Lokanath, N.K. *N*-[2-(5-bromo-2-chloro-pyrimidin-4-yl)thio]-4-methoxy-phenyl]-4-chlorobenzenesulfonamide: The existence of H-bond and halogen bond interactions assisted supramolecular architecture—A quantum chemical investigation. *J. Mol. Struct.* **2022**, *1267*, 133476. [[CrossRef](#)]
13. Koshevoy, I.O.; Krause, M.; Klein, A. Non-Covalent Intramolecular Interactions through Ligand-Design Promoting Efficient Luminescence from Transition Metal Complexes. *Coord. Chem. Rev.* **2020**, *405*, 213094. [[CrossRef](#)]
14. Alkorta, I.; Elguero, J.; Frontera, A. Not Only Hydrogen Bonds: Other Noncovalent Interactions. *Crystals* **2020**, *10*, 180. [[CrossRef](#)]
15. Kumagai, H.; Yagishita, S.; Kanazashi, K.; Ishii, M.; Hayami, S.; Konaka, H.; Ishikawa, R.; Kawata, S. Hydrogen-Bonding Assembly of Coordination Polymers Showing Reversible Dynamic Solid-State Structural Transformations. *Inorganics* **2018**, *6*, 115. [[CrossRef](#)]
16. Siu, S.K.-L.; Po, C.; Yim, K.-C.; Au, V.K.-M.; Yam, V.W.-W. Synthesis, characterization and spectroscopic studies of luminescent *L*-valine modified alkynyl-based cyclometalated gold(III) complexes with gelation properties driven by π – π stacking, hydrogen bonding and hydrophobic–hydrophobic interactions. *Cryst. Eng. Comm.* **2015**, *17*, 8153–8162. [[CrossRef](#)]
17. Wang, R.; Dols, T.S.; Lehmann, C.W.; Englert, U. The halogen bond made visible: Experimental charge density of a very short intermolecular Cl \cdots Cl donor–acceptor contact. *Chem. Commun.* **2012**, *48*, 6830–6832. [[CrossRef](#)]
18. Biradha, K.; Goswami, A.; Moi, R. Coordination polymers as heterogeneous catalysts in hydrogen evolution and oxygen evolution reactions. *Chem. Commun.* **2020**, *56*, 10824–10842. [[CrossRef](#)]
19. Lin, L.; Zhang, Q.; Ni, Y.; Shang, L.; Zhang, X.; Yan, Z.; Zhao, Q.; Chen, J. Rational design and synthesis of two-dimensional conjugated metal-organic polymers for electrocatalysis applications. *Chem* **2022**, *8*, 1822–1854. [[CrossRef](#)]
20. Pachisia, S.; Gupta, R. Architectural and catalytic aspects of designer materials built using metalloligands of pyridine-2,6-dicarboxamide based ligands. *Dalton Trans.* **2020**, *49*, 14731–14748. [[CrossRef](#)]
21. Kuwamura, N.; Konno, T. Heterometallic coordination polymers as heterogeneous electrocatalysts. *Inorg. Chem. Front.* **2021**, *8*, 2634. [[CrossRef](#)]
22. Liu, Q.-Q.; Wang, X.-L.; Lin, H.-Y.; Chang, Z.-H.; Zhang, Y.-C.; Tian, Y.; Lu, J.-J.; Yu, L. Two new polyoxometalate-based metal-organic complexes for the detection of trace Cr(VI) and their capacitor performance. *Dalton Trans.* **2021**, *50*, 9450–9456. [[CrossRef](#)] [[PubMed](#)]
23. Singh, J.; Panda, S.K.; Singh, A.K. Recent developments in supramolecular complexes of azabenzenes containing one to four N atoms: Synthetic strategies, structures, and magnetic properties. *RSC Adv.* **2022**, *12*, 18945–18972. [[CrossRef](#)] [[PubMed](#)]
24. Mylonas-Margaritis, I.; Gérard, A.; Skordi, K.; Mayans, J.; Tasiopoulos, A.; McArdle, P.; Papatriantafyllopoulou, C. From 1D Coordination Polymers to Metal Organic Frameworks by the Use of 2-Pyridyl Oximes. *Materials* **2020**, *13*, 4084. [[CrossRef](#)] [[PubMed](#)]
25. Adonin, S.A.; Novikov, A.S.; Chernova, K.V.; Vinnik, D.A.; Taskaev, S.V.; Korolkov, I.V.; Ilyina, E.V.; Pavlov, A.A.; Novikov, V.V.; Sokolov, M.N.; et al. Heteroleptic copper(II) complexes with 2-bromo-5-methylpyridine: Structures, features of non-covalent interactions and magnetic behavior. *Inorg. Chim. Acta* **2020**, *502*, 119333. [[CrossRef](#)]
26. Zhang, Z.-Y.; Zhang, G.-D.; Sheng, X.-X.; Ding, Q.-W.; Bai, Y.-Z.; Su, Y.; Liu, H.-K.; Su, Z. Efficient MO Dye Degradation Catalyst of Cu(I)-Based Coordination Complex from Dissolution-Recrystallization Structural Transformation. *Cryst. Growth Des.* **2021**, *21*, 333–343. [[CrossRef](#)]
27. Chen, X.; Yang, F.; Han, C.; Han, L.; Wang, F.; Jin, G.; Wang, H.; Ma, J. [Fe₂S₂–Ag_x]-Hydrogenase Active-Site-Containing Coordination Polymers and Their Photocatalytic H₂ Evolution Reaction Properties. *Inorg. Chem.* **2022**, *61*, 13261–13265. [[CrossRef](#)]
28. Hornberger, L.-S.; Adams, F. Photocatalytic CO₂ Conversion Using Metal-Containing Coordination Polymers and Networks: Recent Developments in Material Design and Mechanistic Details. *Polymers* **2022**, *14*, 2778. [[CrossRef](#)]
29. Soldevila-Sanmartín, J.; Calvet, T.; Font-Bardia, M.; Domingo, C.; Ayllón, J.A.; Pons, J. Modulating *p*-hydroxycinnamate behavior as a ditopic linker or photoacid in copper(II) complexes with an auxiliary pyridine ligand. *Dalton Trans.* **2018**, *47*, 6479–6493. [[CrossRef](#)]
30. Vittal, J.J.; Quah, H.S. Photochemical reactions of metal complexes in the solid state. *Dalton Trans.* **2017**, *46*, 7120–7140. [[CrossRef](#)]
31. Garai, M.; Biradha, K. One-Dimensional Coordination Polymers of Bis(3-pyridylacrylamido)ethane: Influence of Anions and Metal Ions on Their Solid State [2 + 2] Photochemical Polymerization and Dimerization Reactions. *Cryst. Growth Des.* **2017**, *17*, 925–932. [[CrossRef](#)]
32. Dong, X.-Y.; Zhang, M.; Pei, R.-B.; Wang, Q.; Wei, D.-H.; Zang, S.-Q.; Fan, Y.-T.; Mak, T.C.W. A Crystalline Copper(II) Coordination Polymer for the Efficient Visible-Light-Driven Generation of Hydrogen. *Angew. Chem. Int. Ed.* **2016**, *55*, 2073–2077. [[CrossRef](#)]
33. Dai, M.; Li, H.-X.; Lang, J.-P. New approaches to the degradation of organic dyes, and nitro- and chloroaromatics using coordination polymers as photocatalysts. *Cryst. Eng. Comm.* **2015**, *17*, 4741–4753. [[CrossRef](#)]
34. Gorai, T.; Schmitt, W.; Gunnlaugsson, T. Highlights of the development and application of luminescent lanthanide based coordination polymers, MOFs and functional nanomaterials. *Dalton Trans.* **2021**, *50*, 770–784. [[CrossRef](#)]
35. Kitagawa, Y.; Tsurui, M.; Hasegawa, Y. Steric and Electronic Control of Chiral Eu(III) Complexes for Effective Circularly Polarized Luminescence. *ACS Omega* **2020**, *5*, 3786–3791. [[CrossRef](#)]

36. Yue, Q.; Gao, E.-Q. Azide and carboxylate as simultaneous coupler for magnetic coordination polymers. *Coord. Chem. Rev.* **2019**, *382*, 1–31. [\[CrossRef\]](#)
37. Castro, I.; Barros, W.P.; Calatayud, M.L.; Lloret, F.; Marino, N.; De Munno, G.; Stumpf, H.O.; Ruiz-García, R.; Julve, M. Dicopper(II) pyrazolenophanes: Ligand effects on their structures and magnetic properties. *Coord. Chem. Rev.* **2016**, *315*, 135–152. [\[CrossRef\]](#)
38. Roy, M.; Adhikary, A.; Debnath, T.; Das, A.K.; Mondal, R. Designing ferromagnetism in Cu(II) complexes using an elusive near-orthogonal bridging mode of the pyrazole ring. *Polyhedron* **2019**, *160*, 46–52. [\[CrossRef\]](#)
39. Tian, Y.; Chen, Y.-Q.; Li, J.; Gao, Q. A Cu(II) coordination framework constructed by the inorganic layer and a bent dipyridyl ligand: Synthesis, structure and magnetic properties. *J. Ind. Chem. Soc.* **2021**, *98*, 100125. [\[CrossRef\]](#)
40. Li, S.-X.; Qiang, J.-W.; Liao, B.-L. Structure, magnetism and oxygen reduction reaction in mixed-valent Cu(I)···Cu(II) complex supported by benzimidazole derivative. *Inorg. Chim. Acta* **2021**, *521*, 120356. [\[CrossRef\]](#)
41. Yang, Y.-Y.; He, M.-Q.; Li, M.-X.; Huang, Y.-Q.; Chi, T.; Wang, Z.-X. Ferrimagnetic copper-carboxyphosphinate compounds for catalytic degradation of methylene blue. *Inorg. Chem. Commun.* **2018**, *94*, 5–9. [\[CrossRef\]](#)
42. Chakraborty, T.; Sarkar, A.; Adhikary, A.; Chakiroy, N.; Das, D. Synthesis of Structurally Diverse Ferrimagnetically and Antiferromagnetically Coupled M^{II} – Mn^{II} ($M = Cu, Ni$) Heterometallic Schiff Base Compounds with a Dicyanamide Spacer and Study of Biomimetic Catalytic Activity. *Cryst. Growth Des.* **2019**, *19*, 7336–7348. [\[CrossRef\]](#)
43. Zordan, F.; Brammer, L. $M-X\cdots X'-C$ Halogen-Bonded Network Formation in $MX_2(4\text{-halopyridine})_2$ Complexes ($M = Pd, Pt$; $X = Cl, I$; $X' = Cl, Br, I$). *Cryst. Growth Des.* **2006**, *6*, 1374–1379. [\[CrossRef\]](#)
44. Nicholas, A.D.; Otten, B.M.; Ayala, G.; Hutchinson, J.; Wojtas, L.; Omary, M.A.; Pike, R.D.; Patterson, H.H. Light-Induced Photochemical Changes in Copper(I) Thiocyanate Complexes Decorated with Halopyridines: Optical Memory Manifestation. *J. Phys. Chem. C* **2017**, *121*, 25430–25439. [\[CrossRef\]](#)
45. Vitorica-Yrezabal, I.J.; Sullivan, R.A.; Purver, S.L.; Curfs, C.; Tang, C.C.; Brammer, L. Synthesis and polymorphism of $(4\text{-ClpyH})_2[CuCl_4]$: Solid–gas and solid–solid reactions. *Cryst. Eng. Comm.* **2011**, *13*, 3189–3196. [\[CrossRef\]](#)
46. Wackerbarth, I.; Widhyadnyani, N.N.A.T.; Schmitz, S.; Stirnat, K.; Butsch, K.; Pantenburg, I.; Meyer, G.; Klein, A. Cu^{II} Complexes and Coordination Polymers with Pyridine or Pyrazine Amides and Amino Benzamides—Structures and EPR Patterns. *Inorganics* **2020**, *8*, 65. [\[CrossRef\]](#)
47. Halcrow, M.A. Jahn–Teller distortions in transition metal compounds, and their importance in functional molecular and inorganic materials. *Chem. Soc. Rev.* **2013**, *42*, 1784–1795. [\[CrossRef\]](#)
48. Kilner, C.A.; McInnes, E.J.L.; Leech, M.A.; Beddard, G.S.; Howard, J.A.K.; Mabbs, F.E.; Collison, D.; Bridgeman, A.J.; Halcrow, M.A. A crystallographic, EPR and theoretical study of the Jahn–Teller distortion in $[CuTp_2]$ ($Tp^- = \text{tris}\{\text{pyrazol-1-yl}\}\text{hydridoborate}$). *Dalton Trans.* **2004**, *2*, 236–243. [\[CrossRef\]](#)
49. Xuan, R.; Li, M.; Wan, Y. Bis(2-chloro-5-methylpyridine- κN)-bis(nitrato- $\kappa^2 O, O'$)copper(II). *Acta Crystallogr. Sect. C Cryst. Struct. Commun.* **2003**, *C59*, m462–m464. [\[CrossRef\]](#)
50. Zhu, H.-B.; Shan, R.-Y.; Yang, W.-N.; Gou, S.-H. From Zero-dimensional to One-dimensional: Use of Metal-Ligand Affinity in Supramolecular Assembly. *Z. Anorg. Allg. Chem.* **2013**, *639*, 125–128. [\[CrossRef\]](#)
51. Puszko, A.; Krojcer, A.; Pełczynska, M.; Wietrzyk, J.; Cieslak-Golonka, M.; Jezierska, J.; Adach, A.; Kubiak, M. Mononuclear copper(II) nitrate complexes with methyl-substituted 4-nitropyridine N-oxide. Physicochemical and cytotoxic characteristics. *J. Inorg. Biochem.* **2010**, *104*, 153–160. [\[CrossRef\]](#)
52. Cameron, A.F.; Forrest, K.P.; Taylor, D.W.; Nuttall, R.H. Structural Investigations of Metal Nitrate Complexes. Part. I. Crystal and Molecular Structure of Bis[dinitratobis(pyridine)copper(II)]-Pyridine $[Cu(NO_3)_2(py)_2]_2$. *Py. J. Chem. Soc. A* **1971**, 2492–2496. [\[CrossRef\]](#)
53. Alvarez, S. A cartography of the van der Waals territories. *Dalton Trans.* **2013**, *42*, 8617–8636. [\[CrossRef\]](#)
54. Steiner, T. The Hydrogen Bond in the Solid State. *Angew. Chem. Int. Ed.* **2002**, *41*, 48–76. [\[CrossRef\]](#)
55. Dey, D.; Bhandary, S.; Thomas, S.P.; Spackman, M.A.; Chopra, D. Energy frameworks and a topological analysis of the supramolecular features in in situ cryocrystallized liquids: Tuning the weak interaction landscape via fluorination. *Phys. Chem. Chem. Phys.* **2016**, *18*, 31811–31820. [\[CrossRef\]](#)
56. Socrates, G. *Infrared and Raman Characteristic Group Frequencies*, 3rd ed.; John Wiley & Sons, Ltd.: New York, NY, USA, 2001; ISBN 9780470093078.
57. Arjunan, V.; Senthilkumari, S.; Ravindran, P.; Mohan, S. Synthesis, FTIR and FT-Raman spectral analysis and structure–activity relations of *N*-(4-bromophenyl)-2,2-dichloroacetamide by DFT studies. *J. Mol. Struct.* **2014**, *1064*, 15–26. [\[CrossRef\]](#)
58. Sambathkumar, K. Analysis of vibrational Spectra of 2-Amino-5-Bromo-4-Methylpyridine Based on Ab Initio and Density Functional Theory Calculations. *Elixir Vib. Spec.* **2016**, *91*, 38381–38391.
59. Warad, I.; Musameh, S.; Badran, I.; Nassar, N.N.; Brandao, P.; Tavares, C.J.; Barakat, A. Synthesis, solvatochromism and crystal structure of *trans*- $[Cu(Et_2NCH_2CH_2NH_2)_2(H_2O)](NO_3)_2$ complex: Experimental with DFT combination. *J. Mol. Struct.* **2017**, *1148*, 328–338. [\[CrossRef\]](#)
60. Harzi, F.; Arfaoui, Y.; Silvestru, C.; Bourguiba, N.F. Synthesis, structural and spectroscopic studies, DFT calculations, thermal characterization and Hirshfeld surface analysis of copper(II) organic-inorganic hybrid material $(C_{12}H_{22}N_2)[CuCl_4]$. *J. Coord. Chem.* **2021**, *75*, 70–83. [\[CrossRef\]](#)

61. Xu, G.C.; Zhang, L.; Liu, L.; Liu, G.F.; Jia, D.Z. Thermal kinetic TG-analysis of the mixed-ligand copper(II) and nickel(II) complexes of *N*-(1-phenyl-3-methyl-4-benzylidene-5-pyrazolone) *p*-nitrobenzoylhydrazide and pyridine. *Thermochim. Acta* **2005**, *429*, 31–42. [CrossRef]
62. Chang, L.-L.; Yang, J.; Lai, S.-Q.; Liu, X.-R.; Yang, Z.-W.; Zhao, S.-S. Synthesis, crystal structures and CT-DNA/BSA binding properties of Co(III) and Cu(II) complexes with bipyridine Schiff base ligand. *Inorg. Chim. Acta* **2022**, *532*, 120751. [CrossRef]
63. Obaleye, J.A.; Lawal, M.; Jadeja, R.N.; Gupta, V.K.; Nnabuike, G.G.; Bamigboye, M.O.; Roy, H.; Yusuff, O.K.; Bhagariya, P. Crystal structure, spectroscopic, DFT calculations and antimicrobial study of the Cu(II) complex bearing second-generation quinolone ofloxacin and 2,2'-bipyridine. *Inorg. Chim. Acta* **2021**, *519*, 120264. [CrossRef]
64. Coey, J.M.D. *Magnetism and Magnetic Materials*; Cambridge University Press: Cambridge, UK, 2010; ISBN 9780521816144.
65. Figgis, B.N.; Lewis, J. The Magnetic Properties of Transition Metal Complexes. In *Progress in Inorganic Chemistry*; Cotton, F.A., Ed.; Wiley: Hoboken, NJ, USA, 1964; Volume 6, p. 177192. [CrossRef]
66. Carlin, R.L.; Burriel, R.; Cornelisse, R.M.; van Duynveldt, A.J. Magnetic Reinvestigation of $[\text{Cu}(\text{C}_5\text{H}_5\text{NO})_2(\text{NO}_3)_2]$: Lack of evidence for a Triplet Ground State. *Inorg. Chem.* **1983**, *22*, 831–832. [CrossRef]
67. Jiang, C.; Luo, Q.; Fu, H.; Lin, H.; Luo, C.; Wang, J.; Meng, X.; Peng, H.; Duan, C.-G.; Chu, J. Ferroelectricity and antiferromagnetism in organic–inorganic hybrid (1,4-bis(imidazol-1-ylmethyl)benzene) $\text{CuCl}_4 \cdot \text{H}_2\text{O}$. *Cryst. Eng. Comm.* **2020**, *22*, 587–592. [CrossRef]
68. Louka, F.R.; Massoud, S.S.; Haq, T.K.; Koikawa, M.; Mikuriya, M.; Omote, M.; Fischer, R.C.; Mautner, F.A. Synthesis, structural characterization and magnetic properties of one-dimensional Cu(II)-azido coordination polymers. *Polyhedron* **2017**, *138*, 177–184. [CrossRef]
69. Kwiatek, D.; Kubicki, M.; Skokowski, P.; Gruszczyńska, J.; Lis, S.; Hnatejko, Z. Five subsequent new pyridine carboxamides and their complexes with d-electron ions. Synthesis, spectroscopic characterization and magnetic properties. *J. Mol. Struct.* **2019**, *1178*, 669–681. [CrossRef]
70. Babu, C.N.; Suresh, P.; Das, P.; Sathyanarayana, A.; Ramadurai, R.; Sampath, N.; Prabusankar, G. Synthesis, crystal structure and spectral properties of copper(II) monomer decorated copper(II) coordination polymer. *J. Mol. Struct.* **2014**, *1062*, 141–146. [CrossRef]
71. Sheldrick, G.M. ShelXT—Integrated space-group and crystal-structure determination. *Acta Crystallogr. Sect. A Found. Crystallogr.* **2015**, *71*, 3–8. [CrossRef]
72. Sheldrick, G.M. *SHELXL-2017/1, Program for the Solution of Crystal Structures*; University of Göttingen: Göttingen, Germany, 2017.
73. Sheldrick, G.M. Crystal structure refinement with SHELXL. *Acta Crystallogr. Sect. C Struct. Chem.* **2015**, *71*, 3–8. [CrossRef]
74. Turner, M.J.; McKinnon, J.J.; Wolff, S.K.; Grimwood, D.J.; Spackman, P.R.; Jayatilaka, D.; Spackman, M.A. *CrystalExplorer17*; University of Western Australia: Crawley, WA, Australia, 2017; Available online: <http://hirshfeldsurface.net> (accessed on 6 January 2020).
75. Turner, M.J.; Grabowsky, S.; Jayatilaka, D.; Spackman, M.A. Accurate and Efficient Model Energies for Exploring Intermolecular Interactions in Molecular Crystals. *J. Phys. Chem. Lett.* **2014**, *5*, 4249–4255. [CrossRef]
76. Mackenzie, C.F.; Spackman, P.R.; Jayatilaka, D.; Spackman, M.A. Crystal Explorer Model Energies and Energy Frameworks: Extension to Metal Coordination Compounds, Organic Salts, Solvates and Open-Shell Systems. *IUCr* **2017**, *4*, 575–587. [CrossRef]

Disclaimer/Publisher's Note: The statements, opinions and data contained in all publications are solely those of the individual author(s) and contributor(s) and not of MDPI and/or the editor(s). MDPI and/or the editor(s) disclaim responsibility for any injury to people or property resulting from any ideas, methods, instructions or products referred to in the content.